1 **Perphenazine-macrocycle conjugates rapidly sequester the Aβ42**
2 **monomer and inhibit amyloid formation**

3 Sarah R. Ball[1], Julius S. P Adamson[2], Michael A. Sullivan[1], Manuela R. Zimmermann[3], Victor Lo[1],
4 Maximo Sanz-Hernandez[4], Frank Jiang[2], Ann H. Kwan[5], Eryn L. Werry[2, 6], Tuomas P. J. Knowles[3, 7],
5 Michael Kassiou[2], Georg Meisl[3], Matthew H. Todd[8*], Peter J. Rutledge[2*] and Margaret Sunde[1*]

6 [1]School of Medical Sciences, The University of Sydney, Sydney, Australia. [2]School of Chemistry, The
7 University of Sydney, Sydney, Australia. [3]Centre for Misfolding Diseases, Department of Chemistry,
8 University of Cambridge, Cambridge UK. [4]Department of Life Sciences, Imperial College London, South
9 Kensington, SW7 2AZ, UK. [5]School of Life and Environmental Sciences, The University of Sydney,
10 Sydney, Australia. [6]Brain and Mind Centre, The University of Sydney. [7]Cavendish Laboratory,
11 University of Cambridge, JJ Thomson Avenue, CB4 0HE, UK. [8]School of Pharmacy, University College
12 London, London UK.

13 *Co-corresponding authors: Margaret Sunde, Peter Rutledge, and Matthew Todd

14 **Email:** margaret.sunde@sydney.edu.au; peter.rutledge@sydney.edu.au; matthew.todd@ucl.ac.uk

15

16

17 **Keywords**

19

20 **Author Contributions**

21 **Conceptualization:** Sarah R. Ball, Julius S. Adamson, Manuela R. Zimmermann, Frank Jiang, Georg
22 Meisl, Matthew H. Todd, Peter J. Rutledge and Margaret Sunde.
23 **Data Curation:** Sarah R. Ball, Julius S. Adamson and Maximo Sanz-Hernandez.
24 **Formal Analysis:** Sarah R. Ball, Michael A. Sullivan, Manuela R. Zimmermann, Maximo Sanz-
25 Hernandez and Georg Meisl.
26 **Funding Acquisition:** Peter J. Rutledge and Margaret Sunde.
27 **Investigation:** Sarah R. Ball, Julius S. Adamson, Michael A. Sullivan, Victor Lo, Maximo Sanz-
28 Hernandez, Frank Jiang, Peter J. Rutledge and Margaret Sunde.
29 **Methodology:** Sarah R. Ball, Julius S. Adamson, Michael A. Sullivan, Manuela R. Zimmermann,
30 Victor Lo, Maximo Sanz-Hernandez, Frank Jiang, Ann H. Kwan, Tuomas P. Knowles, Georg Meisl,
31 Eryn L. Werry, Matthew H. Todd, Peter J. Rutledge and Margaret Sunde.
32 **Project Administration:** Peter J. Rutledge and Margaret Sunde.
33 **Resources:** Michael Kassiou, Peter J. Rutledge and Margaret Sunde.
34 **Supervision:** Ann H. Kwan, Tuomas P. Knowles, Eryn L. Werry, Michael Kassiou, Matthew H. Todd,
35 Peter J. Rutledge and Margaret Sunde.
36 **Validation:** Sarah R. Ball, Julius S. Adamson, Frank Jiang and Margaret Sunde.
37 **Visualization:** Sarah R. Ball, Julius S. Adamson, Michael A. Sullivan, Manuela R. Zimmermann,
38 Maximo Sanz-Hernandez, Georg Meisl, Peter J. Rutledge and Margaret Sunde.
39 **Writing - Original Draft Preparation:** Sarah R. Ball, Julius S. Adamson, Michael A. Sullivan, Peter J.
40 Rutledge and Margaret Sunde.
41 **Writing - Review & Editing:** Sarah R. Ball, Julius S. Adamson, Michael A. Sullivan, Manuela R.
42 Zimmermann, Victor Lo, Maximo Sanz-Hernandez, Ann H. Kwan, Tuomas P. Knowles, Georg Meisl,
43 Eryn L. Werry, Michael Kassiou, Matthew H. Todd, Peter J. Rutledge and Margaret Sunde.

44 **Abstract**

45 Alzheimer's disease is imposing a growing social and economic burden worldwide and effective
46 therapies are required. Strategies aimed at the removal of fibrillar plaques formed by the amyloid-β
47 peptide have not proved therapeutic and the focus has shifted to approaches that target the cytotoxic
48 oligomeric amyloid-β species that are populated before fibrils are deposited. We have designed and
49 synthesized perphenazine-cyclam conjugates that specifically and rapidly bind to the monomeric form
50 of Aβ42, reducing the production of both cytotoxic oligomers and amyloid fibrils. We have applied
51 detailed kinetic analysis and NMR spectroscopy to show that the perphenazine-cyclam conjugates
52 divert the Aβ42 monomer into amorphous aggregates that are not toxic to differentiated SH-SY5Y cells
53 *in vitro.* Unlike most other amyloid inhibitors studied to date, these conjugates inhibit oligomer and fibril
54 assembly even in the presence of pre-formed fibrillar seeds, demonstrating that they act through a
55 monomer sequestration mechanism. These modular, three-dimensional conjugates therefore
56 effectively prevent monomer-dependent secondary nucleation, the autocatalytic process that generates
57 the majority of toxic oligomers.

58

59

60   **Introduction**

61   Alzheimer's disease (AD) is the most common form of dementia and one of the most devastating
62   diseases of the current age. There are currently no approved disease-modifying therapies for this
63   neurodegenerative disease. Although the full sequence of critical molecular events that lead to neuronal
64   death is yet to be defined, self-assembly of the amyloid-β peptide (Aβ) into soluble oligomers and
65   amyloid fibrils has been shown to generate neurotoxic oligomeric species[1-3]. These oligomers impact
66   neuronal activity through effects on cell membranes, calcium homeostasis, and glutamate reuptake,
67   amongst other deleterious mechanisms[4-10]. The failure of clinical trials aimed at reducing the
68   accumulation of mature Aβ fibrils in extracellular plaques has seen efforts shift towards intervention at
69   earlier stages in the pathway, with the aim of inhibiting formation of these toxic, pre-fibrillar oligomers[11].

70   Aβ amyloid formation is a complex, multiple-step process, initiated by primary nucleation from Aβ
71   monomers. This is followed by recruitment of additional monomers, leading to the formation of multiple
72   different soluble oligomers with a range of sizes and toxicities[12]. As amyloid fibrils form, they offer sites
73   for elongation at their ends, and for secondary nucleation on their lateral surfaces[13, 14], generating
74   further oligomeric species. Monomer-dependent secondary nucleation is a significant source of
75   cytotoxic oligomeric Aβ42 species and is the dominant nucleation process even in cerebrospinal fluid
76   and the presence of phospholipid membranes[15].

77   Effective inhibition of Aβ-associated toxicity is likely to require a mechanism that is effective against all
78   steps of the pathway[16]. Several small-molecule compounds have been shown to suppress primary
79   nucleation or to accelerate fibril formation[17-19] and have shown promise in animal models but are yet to
80   show efficacy in clinical trials[20]. Some small molecules increase the population of neurotoxic Aβ
81   oligomers[21] and other proposed inhibitors are not effective in the presence of pre-formed fibrils[17, 22]. The
82   molecular chaperone domain pro-SPC and certain antibody fragments are inhibitors of secondary
83   nucleation[23, 24], as are some small molecules[18, 25]. The efforts to identify effective modulators of the Aβ
84   assembly process have been hampered by the use of poorly characterised preparations of the peptide
85   and by testing against Aβ40, the less amyloidogenic and less clinically relevant isoform, rather than
86   Aβ42 [26-28]. The growing impact of AD necessitates continued efforts directed at the development of
87   therapeutic modulators.

88   We have shown previously that cyclam derivatives with triazole-linked pendant groups can adopt a
89   range of different, defined pendant geometries depending on the connectivity of the triazole linker and
90   the metal ion coordinated by the macrocycle[29-31]. Combining these insights with the documented
91   capacity of polymeric perphenazine conjugates to modulate Aβ aggregation[28], we designed a series of
92   molecules in which cyclam is linked via click-derived triazoles to pendant groups that are known to
93   interact with Aβ42.

94   Quantitative kinetic analysis demonstrates that this series of molecules effectively and rapidly
95   sequesters the monomeric form of Aβ42. We show that this monomer sequestration activity inhibits all
96   downstream events that are dependent on monomer concentration, including suppression of the
97   formation of toxic oligomers and amyloid fibril assembly, even in the presence of preformed fibril seeds.
98   These novel molecules redirect the Aβ42 formation pathway towards the generation of amorphous
99   aggregates that are not toxic to differentiated, neuron-like SH-SY5Y cells. This study provides the first
100   demonstration of a reduction in neurotoxicity resulting from the designed diversion of the Aβ42
101   monomer into non-toxic oligomers.

102   **Results**

103   **Perphenazine-cyclam conjugates inhibit Aβ42 amyloid assembly**

104   A series of cyclam conjugates was designed to enable a systematic investigation of the Aβ aggregation
105   and amyloid assembly pathways. Six parent cyclam derivatives were prepared: the mono-substituted
106   naphthyl (**C1**), dopamine (**C4**) and perphenazine (**C7**) analogues, and corresponding bis-substituted
107   compounds with naphthyl (**C10**), dopa (**C13**) and perphenazine (**C16**) pendants, along with their zinc(II)

3

108 and copper(II) complexes (mono-naphthyl **C2**, **C3**; mono-dopa **C5**, **C6**; mono-perphenazine **C8**, **C9**;
109 bis-naphthyl **C11**, **C12**; bis-dopa **C14**, **C15**; and bis-perphenazine **C17**, **C18**) (Fig. 1A and SI Fig. S1A).
110 Initial screening of these compounds showed the bis-perphenazine derivative (ligand **C16)** to have
111 promising capacity to suppress amyloid formation by both Aβ40 and Aβ42 (SI, Fig. S1B and C).

112 We prepared the bis-perphenazine ligand (**C16**) and its zinc (**C17**) and copper (**C18**) analogues and
113 determined the ability of these three cyclam conjugates to inhibit amyloid formation by Aβ42 (SI, Fig.
114 S1C,D). We have characterised the inhibitory activity of the molecules against Aβ42 amyloid assembly.
115 This isoform is clinically associated with an increase in amyloid deposition[32] and we have utilised highly
116 purified, monomeric recombinant Aβ42, prepared using the methods of Linse and colleagues[33, 34]. Aβ42
117 prepared according to these protocols displays highly reproducible kinetics of amyloid assembly. The
118 three cyclam conjugates **C16**, **C17** and **C18** were found to be potent inhibitors of Aβ42 amyloid
119 formation, as monitored by ThT fluorescence (Fig. 1; SI Fig. S2 and Fig. S3).
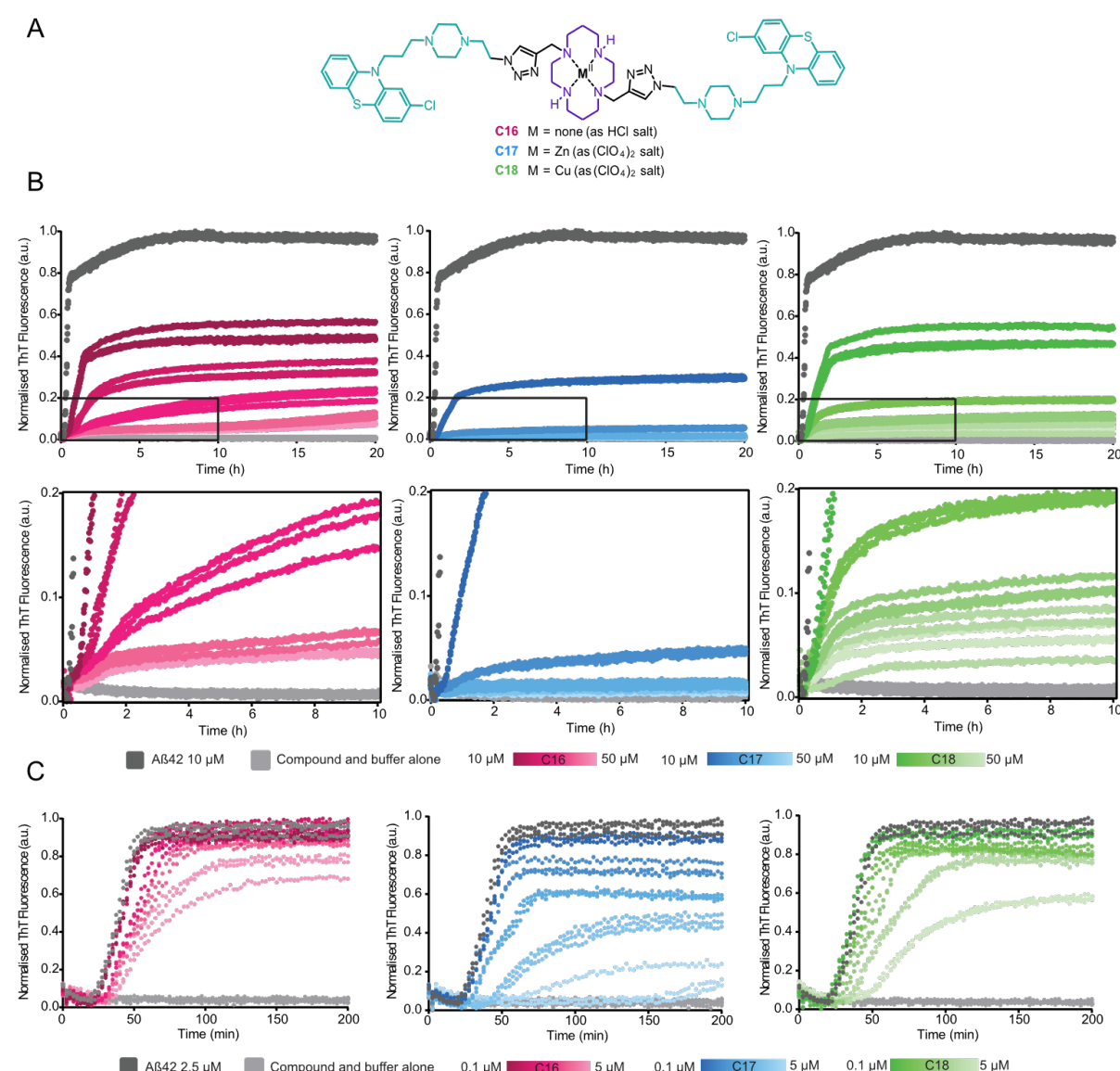

122 **Fig. 1.** Time courses of fibril formation by Aβ42 show concentration-dependent inhibition of aggregation
123 by **C16**, **C17** and **C18**. *(A)* The lead compounds used in this study combine a cyclam macrocycle
124 (purple) with pendant perphenazine moieties (cyan), conjugated via a click-derived triazole (black), and
125 deployed either as the unmetallated HCl salt **C16**, the zinc perchlorate complex **C17**, or the copper(II)
126 perchlorate **C18**. *(B)* 10 μM monomeric Aβ42 in the absence or presence of either 1% DMSO (dark
127 grey) or 10 – 50 μM of **C16** (pink), **C17** (blue) and **C18** (green). Lower section displays an enlarged 10-

4

128 hour window. N = 3 (SI Fig S2). *(C)* 2.5 µM monomeric Aβ42 in the presence of either 1% DMSO (dark
129 grey) or 0.1, 1, 2, 3 or 5 µM of compounds. N = 4 (SI Fig S3). All samples were measured in triplicate
130 under quiescent conditions at 37 °C. Traces have been corrected for time zero and data normalised as
131 a function of the maximum fluorescence intensity, using GraphPad Prism.

132

133 The inhibitors demonstrated a concentration-dependent effect, and at a 1:5 molar ratio of
134 Aβ42:compound, using 10 µM Aβ42, amyloid assembly was almost completely suppressed, as judged
135 by the reduction in the level of Thioflavin T (ThT) fluorescence observed (Fig. 1B). Assays at lower
136 Aβ42 concentration, using a range of inhibitor concentrations that allowed the plateau phase of amyloid
137 assembly to be reached, revealed that all three compounds also introduce an increase in lag phase.
138 The length of the lag phase increases with increasing inhibitor concentration (Fig. 1C). The zinc(II)
139 complex **C17** displayed the strongest inhibition, followed by copper(II) complex **C18**, and the
140 uncomplexed ligand **C16**, highlighting the capacity of the central metal ion to influence the
141 three-dimensional shape of the inhibitor – in particular the relative orientation of the two pendant groups
142 [29, 30, 35] – and resulting impact on the mechanism of Aβ42 amyloid inhibition. The exact nature of this
143 inferred variation in shape between **C16**, **C17** and **C18** remains to be elucidated.

144 Perphenazine alone does not display strong inhibition of Aβ42 amyloid formation under these
145 conditions, highlighting the fact that it is not the perphenazine moiety *per se* that is responsible for the
146 inhibitory activity (SI Fig. S4). The observed inhibition is also not due to an effect of unchelated metal
147 ions directly on Aβ42. Previous studies have demonstrated that Zn(II) and Cu(II) cations can themselves
148 inhibit Aβ42 amyloid formation[36-38], reflected by an increase in the lag phase or a decrease in the
149 observed ThT intensity (SI Fig. 5A). However, we observed that **C17** and **C18** remain effective inhibitors
150 of Aβ amyloid formation even in the presence of the chelating agent EDTA, which would sequester any
151 free metal ions and block their inhibitory capacity (SI Fig. 5B).

152 **The perphenazine conjugates divert Aβ42 from amyloid assembly towards amorphous**
153 **aggregates**

154 A sensitive protein concentration assay confirmed that when the plateau of assembly was reached, in
155 samples containing Aβ42 only, or Aβ42 in the presence of a 5-fold molar excess of inhibitor, all Aβ42
156 was converted to an insoluble form that was readily pelleted by centrifugation (SI Fig. S6). Transmission
157 electron microscopy was used to examine the final morphology of the Aβ42 material present after ~40 h
158 incubation with compounds or 1% DMSO as control. An inhibitor concentration dependent shift from
159 the characteristic fibrillar morphology of Aβ42 amyloid (Fig. 2A) to amorphous aggregates (Fig. 2B, C
160 & D) was observed. The amorphous aggregates had a beads-on-a-string appearance, with the "beads"
161 approximately 20 nm wide and the "strings" >1 µm in length. Only amorphous material was observed
162 when Aβ42 was incubated in the presence of **C16**, even at 1:1 molar ratio of **C16**:Aβ42, while a
163 combination of fibrillar and amorphous material was observed in samples prepared at 1:1 molar ratios
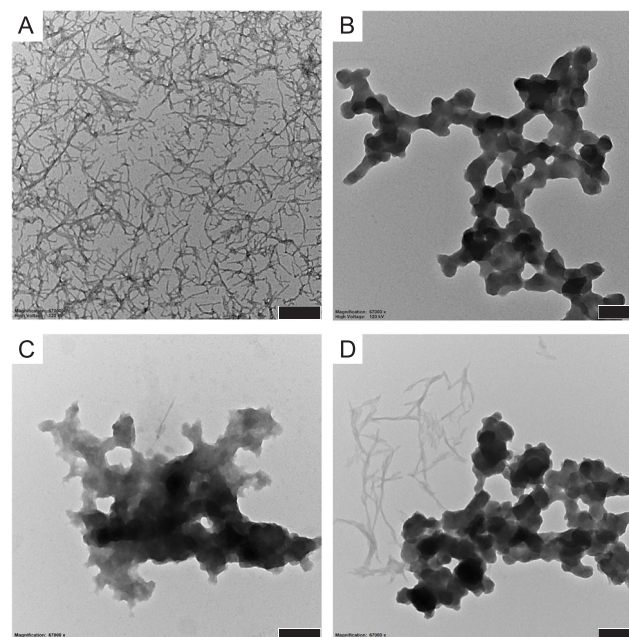164 of **C17**:Aβ42 and **C18**:Aβ42 (SI Fig. S7).

5

Fig. 2. Transmission electron microscopy images showing representative examples of the morphology of fibrils formed by 10 µM Aβ42 alone (A) or aggregates formed by 10 µM Aβ42 in the presence of 50 µM **C16** (B), **C17** (C) and **C18** (D). Scale bar represents 200 nm.

The perphenazine conjugates reduce neurotoxicity associated with Aβ oligomers

Many groups have demonstrated that soluble intermediate species formed by Aβ42 *in vitro* are neurotoxic[1-3, 39]. Accordingly, the ability of compounds **C16**–**C18** to prevent the formation of toxic Aβ42 species was indexed using SH-SY5Y cells which had been differentiated to an AD-appropriate phenotype by treatment with retinoic acid and brain-derived neurotrophic factor[40]. Lyophilised, monomeric Aβ42 was treated with hexafluoro-2-propanol (HFIP), lyophilised, and then resuspended in PBS, before being diluted in cell media and added immediately to cells. Aβ42 fibrils were prepared by incubating monomeric Aβ42 solution in cell media at 37 °C for 24 hours, a time point significantly past the plateau level in unshaken ThT experiments using cell media (SI Fig. S8). The compounds were added to differentiated SH-SY5Y cells alone or added together with Aβ42 in a monomeric or fibrillar form. After 24 hours, the number of metabolically-active cells was measured using a CTB fluorescence assay. The CellTiter-Blue® (CTB) assay of cell viability was chosen, given published concerns regarding the use of MTT with Aβ42[1].

By themselves, compounds **C16**, **C17** and **C18** displayed no significant toxicity towards differentiated SH-SY5Y cells, relative to vehicle only (Fig. 3A). Exposure of these cells to freshly prepared monomeric Aβ42 resulted in significant ($P < 0.001$) toxicity compared to vehicle, as expected due to the generation of oligomeric species, while the addition of **C16**, **C17** or **C18** led to significant protection against this neurotoxicity (Fig. 3B). Perphenazine was not cytotoxic by itself and imparted a similar level of protection as **C16**, **C17** and **C18**. These results contrast with the observed neurotoxicity of epigallocatechin gallate (EGCG) at the same concentrations and the lack of protection by this polyphenol against cytotoxicity induced by addition of monomeric Aβ42 (Fig. 3A,B). When Aβ42 was prepared in fibrillar form and then added to cells, no cytotoxicity was observed with fibrils alone or in the presence of compounds (Fig. 3C). Following from these experiments, independent concentration response assays were performed with **C16**. The IC_{50} for **C16** was determined to be 2.33 µM (n = 3; SD = 0.89) (Fig. 3D). Here we have used an established assay of neurotoxicity, with differentiated SH-SY5Y cells and well-characterised preparations of monomeric and fibrillar Aβ42. Although the origins of the neurotoxicity resulting from the conversion of Aβ42 from monomeric to fibrillar form *in vitro* are

6

198   not defined, these results provide clear evidence that the generation of amorphous Aβ42 aggregates in
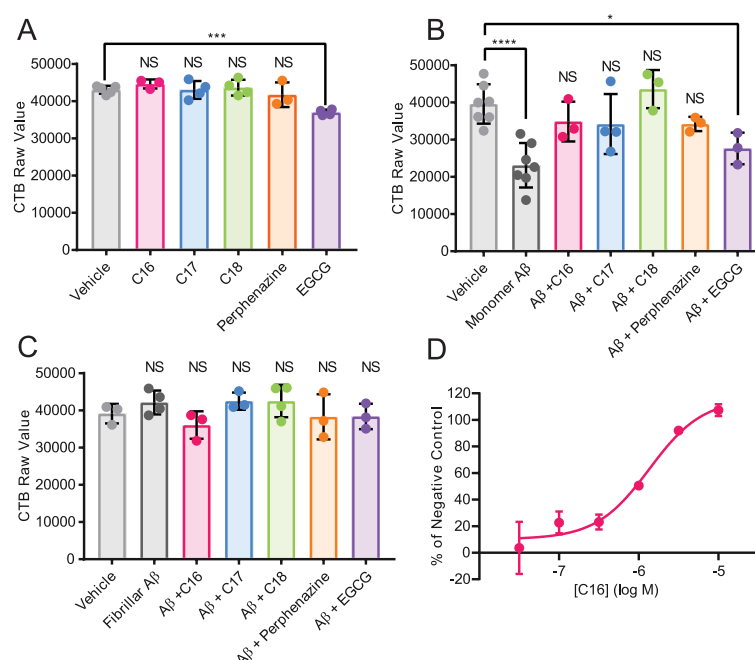199   the presence of **C16**–**C18** prevents the formation of neurotoxic species.

200
201   **Fig. 3.** Cell viability was measured using the CellTiter Blue® assay after 24 h incubation with vehicle or
202   10 μM compound, with or without 20 μM Aβ42. (*A*) Compounds alone. (*B*) Compounds incubated with
203   monomeric Aβ42. (*C*) Compounds incubated with fibrillar Aβ42. The figure displays the mean ± SD of
204   N ≥ 3 independent experiments. One-way ANOVA followed by a Bonferroni's multiple comparisons test
205   at the 0.05 level was used to determine the difference between each condition and vehicle control (****
206   $p < 0.0001$, *** $p < 0.001$, * $p < 0.05$, NS = non-significant). (*D*) Representative concentration-response
207   curve for **C16** incubated with Aβ42 showing mean ± SD of duplicates. IC_{50} = 2.33 μM (SD = 0.89). N =
208   3.

209
210   **C16, C17 and C18 inhibit Aβ amyloid formation through sequestration of Aβ42 monomers**

211   The microscopic processes underlying amyloid formation of Aβ42 are primary nucleation, elongation
212   and secondary nucleation[41, 42]. Their relative importance can be quantified through their rate constants,
213   obtained by fitting integrated rate laws within the framework of chemical kinetics[43]. Data measured at
214   2.5 μM and 10 μM Aβ42, in the presence of a range of concentrations of inhibitor, were analysed using
215   the online fitting software AmyloFit. The rate constants of the unperturbed systems agreed well with
216   similar experiments[13]. To probe the mechanism of action of the inhibitory compounds **C16**, **C17** and
217   **C18**, we varied systematically one rate constant in the rate law, or the level of available monomer,
218   respectively[43]. By comparing how well these modified rate laws can describe the data, a mechanism
219   that primarily involves inhibition of primary nucleation could be ruled out for **C16**, **C17** and **C18** (Fig. 4A,
220   B and SI Fig. S9-13) as the origin of the changes in the kinetic behaviour in the presence of the inhibitor.
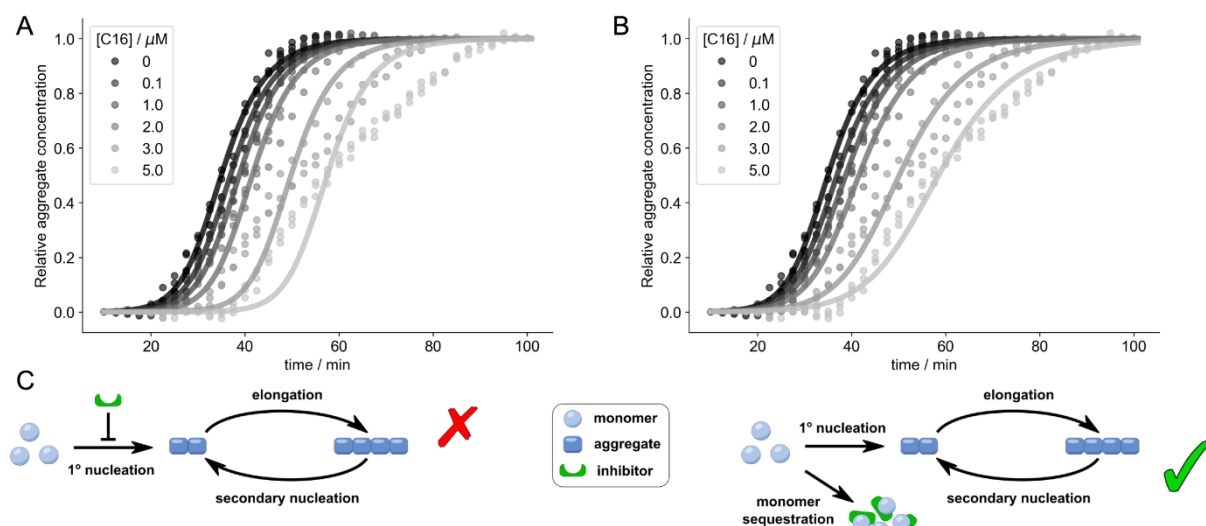
7

Fig. 4. Chemical kinetics analysis reveals inhibition through monomer sequestration. To elucidate the major mechanism of inhibition, normalised aggregation curves measured in thioflavin T fluorescence assays were fitted under the constraint that deviation from the unperturbed system was allowed in only one microscopic step or the free monomer concentration, respectively. Representative curves shown in A and B, all fits shown in the SI. *(A)* The observed inhibition cannot be described through inhibition of primary nucleation. *(B)* Inhibition through monomer sequestration is a plausible mechanism based on the kinetic profiles. *(C)* Microscopic steps underlying amyloid formation, with the suggested mode of inhibition through monomer sequestration.

The introduction of small numbers of preformed fibril seeds at the beginning of the aggregation reaction can be used to bypass primary nucleation. These compounds remain effective as inhibitors of Aβ42 amyloid fibril formation even when exogenous fibril seeds are present (Fig. 5). In the presence of 2% or 5% seeds, and the presence of **C16–C18** at 1:2.5 or 1:5 Aβ42:compound molar ratio resulted in inhibition of Aβ42 assembly, similar to the level of inhibition observed in the absence of pre-formed seeds (Fig. 5 and SI Fig. S14). In addition to ruling out the blocking of primary nucleation as the source of the inhibitory effect, the results observed in the presence of seeds, when the aggregation reaction reaches completion much sooner, suggest that binding of the compounds to the monomeric form of Aβ42 occurs rapidly.
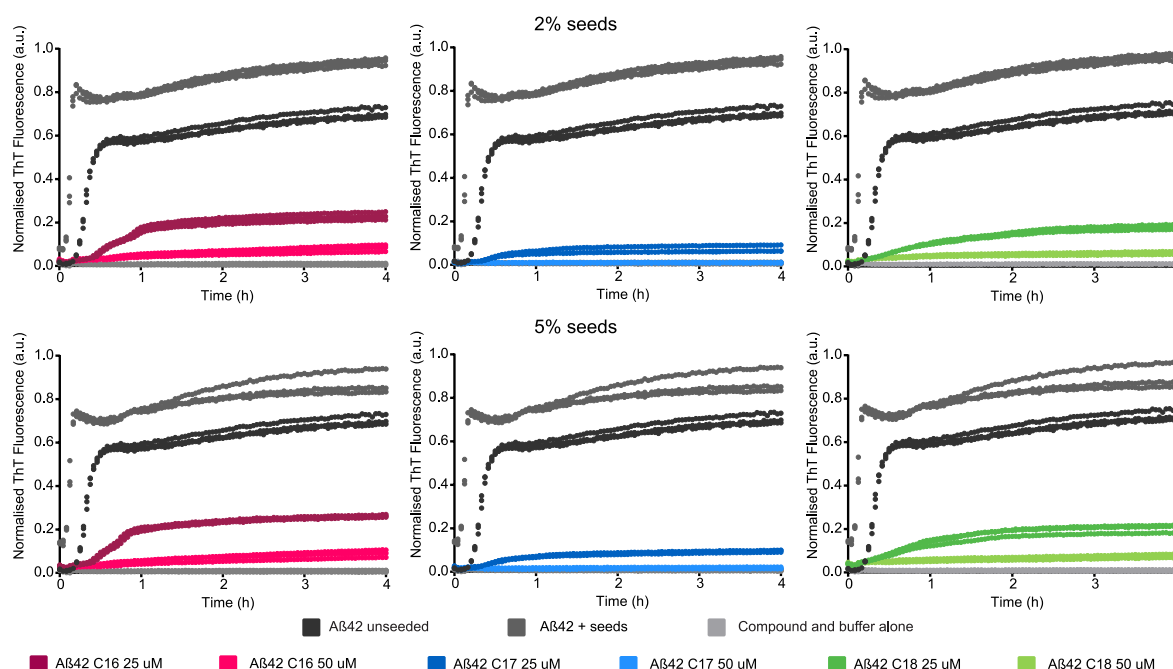
8

Fig. 5 Characterisation of the effects of compounds on seeded Aβ42 aggregation. 10 μM monomeric Aβ42, in the absence of seeds (black) or presence of 2% (top panel) or 5% (bottom panel) seeds and 1% DMSO (dark grey), 25 or 50 μM of compounds. N = 3 (SI Figs S14). All samples were measured in triplicate under quiescent conditions at 37 °C. Traces have been corrected for time zero and data normalised as a function of the maximum fluorescence intensity, using GraphPad Prism.

Based on the fits to the normalised kinetic data alone, mechanisms based on inhibition of secondary nucleation, inhibition of elongation, and monomer sequestration were similarly likely as the main modes of action of compounds **C16**–**C18** (SI Fig. S9-13). However, we found a clear correlation between the ThT intensity at completion of the aggregation reaction and the effective monomer concentration determined from the fits (Fig. 6A, B, C insets). As the fitting was performed on normalised kinetic data, these two quantities constitute independent measures of the same physical property. The correlation between an equilibrium measure, the plateau level, and a parameter estimated on the basis of normalised kinetics, the effective monomer concentration, provides further independent evidence for monomer sequestration by these inhibitors. In addition to accounting for the delay in aggregation and decrease in ThT signal, monomer sequestration by the inhibitors also provides a mechanistic explanation for the appearance of amorphous material as discussed above. These fits were made assuming that this monomer sequestration proceeds much faster than aggregation and can thus be modelled by a reduced effective monomer concentration.

Further support for monomer sequestration as the dominant mode of inhibition of Aβ42 aggregation by **C16**, **C17** and **C18** was gained by obtaining consistent values for the apparent dissociation constant of monomer and inhibitor, K_D, by orthogonal methods. First, the effective monomer concentration obtained through the chemical kinetics analysis at different monomer and inhibitor concentrations was used to construct monomer-inhibitor binding curves (Fig. 6A, B, C). To fit these data, we assumed a simple one-to-one binding, yielding K_D values of 7.6 μM (95% CI, 6.6–9.1) for **C16**, 5.7 μM (95% CI, 4.6–7.1) for **C17** and 7.4 μM (95% CI, 6.2–9.1) for **C18**.

Secondly, we utilised one-dimensional ^{1}H NMR spectroscopy to determine an apparent binding constant for the interaction between the inhibitors and Aβ42. For each of **C16**, **C17** and **C18**, inhibitor was titrated into a solution containing 10 μM unlabelled Aβ42, over the inhibitor concentration range of 1–50 μM. A decay profile in the protein signal intensity across the spectrum was observed with increasing concentration of all three inhibitors (Fig. 6 and SI Fig. S15). A 5:1 ratio of inhibitor:Aβ42 resulted in a reduction of proton signals to baseline, consistent with the sequestration of monomer into

9

273 very large and/or insoluble assemblies, the precipitation of material during the course of the NMR
274 titrations, and the amorphous aggregates observed by TEM (Fig. 3). The signal decay curves were
275 fitted to a quadratic equation for the calculation of the apparent K_D of each compound, yielding 4.6 μM
276 (95% CI, 3.1–6.5) for **C16**, 3.4 μM (95% CI, 2.2–4.9) for **C17** and 3.7 μM (95% CI, 2.4–5.3) for **C18**.
277 The observed effect of these perphenazine cyclam conjugates on Aβ42 assembly is different to that of
278 the polyphenol EGCG, where the presence of EGCG results in only a small decrease in the intensity of
279 the observed 1H spectrum from Aβ42, up to 31% signal loss at a 5-fold excess of small molecule (Fig.
280 6D and SI Fig. S15). This is evidence that upon addition of EGCG, the monomeric Aβ42 species is still
281 the most prevalent in the sample. In contrast, when the less aggregation-prone Aβ40 interacts with
282 EGCG, specific interactions are observed by solution NMR and it forms insoluble oligomers that are in
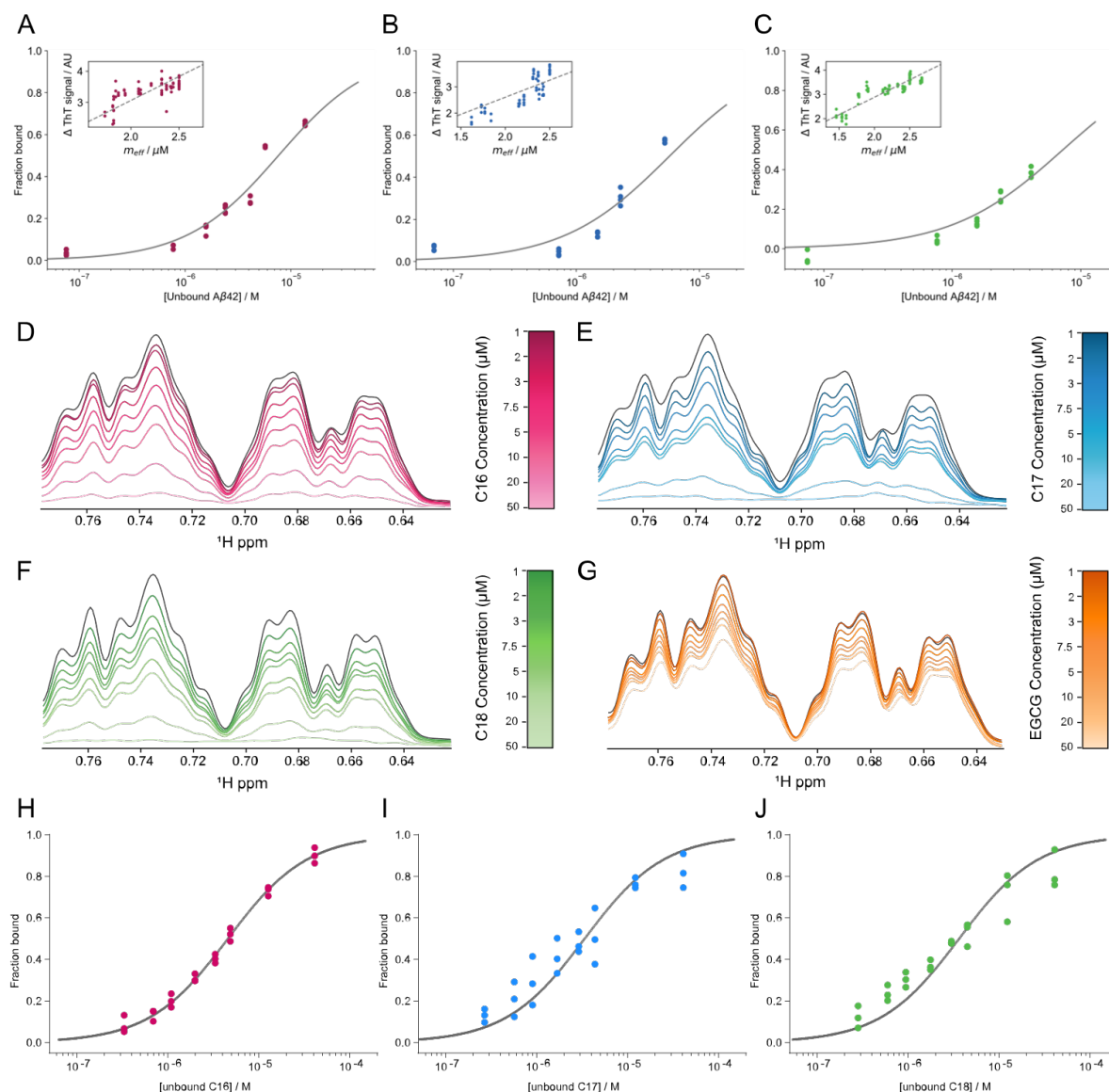283 equilibrium with soluble Aβ40[44].

284

285
286 **Fig. 6.** Dissociation constants determined from ThT assays and ¹H NMR. Monomer-inhibitor binding
287 curves for *(A)* **C16**, *(B)* **C17** and *(C)* **C18**, with correlation between the effective free monomer
288 concentration and the absolute increase in ThT signal shown as insets. One-dimensional ¹H NMR
289 spectroscopy to determine apparent K_D for compounds. Unlabelled 10 μM Aβ42 (dark grey) was
290 incubated with 1–50 μM *(D)* **C16,** *(E)* **C17**, *(F)* **C18** and *(G)* **EGCG**, and spectra recorded at 4 °C. Methyl
291 proton region is displayed, all regions analysed are shown in SI Fig. 15. Increasing concentration of

10

292 **C16**–**C18** resulted in a decay in protein signal intensity. Binding curves for *(H)* **C16,** *(I)* **C17** and *(J)* **C18**
293 constructed from signal decay curves and used to calculate the apparent K_D.

294

295 A monomeric sample of recombinant ^{15}N-labeled Aβ42 was prepared and analysed in the absence and
296 presence of **C16** to probe the regions of the polypeptide involved in the interaction. The ^{15}N HSQC
297 spectrum collected in the absence of any added compound reflected the high quality of the recombinant,
298 monomeric Aβ42 sample and the chemical shifts were superimposable upon those reported by others
299 previously for Aβ42[45] (SI Fig. S16). Addition of **C16** resulted in an immediate reduction in signal intensity
300 that was uniform across all peaks in the spectrum. Protein that is not sequestered into an amorphous
301 aggregate remains in the solution at the 1:1 ratio of protein:inhibitor. No peak-specific changes in signal
302 intensity or chemical shift were detected that could be attributed to binding of **C16** to a distinct region
303 of monomeric Aβ42. Instead, the loss of signal is consistent with the binding of monomer to **C16**
304 resulting in the generation of a conformation that is highly aggregation-prone and rapidly forms large
305 structures, undetectable by solution NMR.

306 **Discussion**

307 We have designed a class of compounds that specifically sequester the monomeric form of Aβ42 into
308 non-fibrillar assemblies that are different to the cytotoxic oligomeric forms associated with Aβ42 amyloid
309 formation. The process by which monomeric Aβ42 converts to the mature fibrillar form detected in
310 amyloid plaques involves multiple oligomeric and prefibrillar species that may act as reactants,
311 products, intermediates, and catalysts of the process and contribute to toxicity to different extents. The
312 ability to interrogate a change in aggregation kinetics caused by an inhibitor, and thereby identify the
313 mechanism of inhibition, offers new opportunities to understand the consequences of intervention at
314 defined points within the Aβ42 assembly pathway. Many studies of peptide-based inhibitors that
315 incorporate "disruption elements" report success in preventing the formation of the β-structure that
316 stabilises amyloid fibrils and can influence elongation[46] and inhibitors have been described that
317 specifically inhibit secondary nucleation[18], but the impact of these interventions on residual Aβ monomer
318 concentration has not always been described. The kinetic theory of protein aggregation inhibition
319 reveals that inhibitors such as the cyclam-perphenazine conjugates described here, which sequester
320 monomeric Aβ42, will reduce the rates of primary nucleation, elongation and secondary nucleation, and
321 are therefore likely to have a large impact on amyloid assembly overall[16].

322 In addressing AD the sequestration of monomer into non-toxic assemblies and consequent reduction
323 of oligomer formation, could be beneficial. Studies of the effect of EGCG on Aβ42 indicate that it
324 converts the peptide to off-pathway oligomers and remodels pre-formed fibrils, although these effects
325 are not rapid[26, 47, 48]. The intrinsically disordered and dynamic nature of monomeric Aβ42 has impeded
326 the use of traditional approaches that focus on identifying chemical moieties that bind to defined sites
327 on the target. Recently a small molecule (10074-G5) that binds to the monomeric form of Aβ42 has
328 been reported[16, 22]. The binding of 10074-G5 to Aβ42, with K_D of ~40 μM, sequesters Aβ42 in its soluble
329 form and reduces its hydrophobicity. In contrast, we observed an immediate uniform reduction in signal
330 intensity across the spectrum when **C16** was added to Aβ42 at a 1:1 ratio, indicating that **C16**
331 sequesters Aβ42 in a polymeric, insoluble assembly. The small molecule 10074-G5 reduces functional
332 deficits in a *C. elegans* model of Aβ42-associated toxicity, however its impact on neuronal toxicity is yet
333 to be reported and it does not display a concentration-dependent inhibition of seeded assembly *in vitro*.
334 Thus, further work is required to define the relative benefit of Aβ42 sequestration in monomeric versus
335 non-toxic oligomeric form.

336 The inventive modular design of the compounds described here offers a toolkit for future elucidation of
337 the key moieties and properties that influence Aβ42 monomer binding and subsequent formation of
338 amorphous aggregates. Compounds that were effective at Aβ42 monomer sequestration protected
339 against Aβ42-induced cytotoxicity. This scaffold provides a base for future rational design of more
340 potent compounds that act through the same mechanism, yet which are accessible via a divergent
341 synthetic strategy. This class of compounds can provide wide mass-to-charge and hydrophobic-to-

342   hydrophilic surface area ratios, while the attachment of both rigid and flexible pendants provides a great
343   diversity of possible interactions with client protein targets. The switchable geometry allows
344   maintenance of a constant periphery while varying the gross molecular shape. Given that self-assembly
345   and aggregation of proteins are three-dimensional processes, this level of structural control has
346   significant potential to contribute to effective inhibition. AD is one of over 50 human disorders considered
347   to be proteinopathies. The critical pathogenic species associated with protein aggregation and amyloid
348   formation in each of these disorders likely have unique features. However, a similar dissection of
349   assembly pathways with modular scaffolds decorated with protein-specific binding moieties may reveal
350   points for therapeutic intervention in other protein aggregation-related diseases.

351

352   **Materials and Methods**

353   **Synthesis of lead compounds C16–C18.**
354   Full synthetic procedures and characterisation data are detailed in the Supporting Information.

355
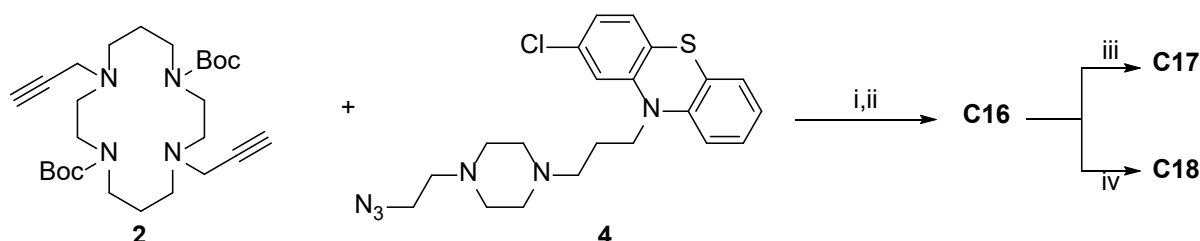
356   **Reaction scheme 1:** Cyclam (1,4,8,11-tetraazacyclotetradecane) **1** was converted to the di-Boc-di-
357   propargyl derivative **2** in 68% yield over four steps using previously reported methods[49, 50].
358   Perphenazine **3** was converted to the azide **4** (79%) by activating its primary alcohol with
359   diphenylphosphoryl azide (DPPA) and displacing with sodium azide in dimethylformamide (DMF). The
360   azide **4** (2 equivalents) and bis-alkyne **2** were coupled using a copper-catalysed azide/alkyne
361   cycloaddition reaction (CuAAC) to yield the protected ligand **5** (46%), before the Boc groups were
362   removed using 4 M HCl in dioxane to afford **C16** (74%). The HCl salt **C16** was converted to its zinc(II)
363   (**C17**) and copper(II) (**C18**) complexes by first treating with Ambersep 900 hydroxide form resin to
364   generate the free amine, then stirring overnight at room temperature with either zinc(II) perchlorate
365   hexahydrate (for **C17**, 63%) or copper(II) perchlorate hexahydrate (for **C17**, 64%). All compounds were
366   dissolved in 100% DMSO and stored at 4 °C until use. Reagents and conditions: i. $CuSO_4.5H_2O$ (0.2
367   equiv.), sodium ascorbate (0.5 equiv.), THF/H_2O (2:3), rt, 16 h, 46%; ii. 4 M HCl in dioxane (excess), 0
368   °C, 1 h, 74%; iii. Ambersep 900 hydroxide form resin, MeOH, 15 min, then $Zn(ClO_4)_2$, MeOH, reflux, 16
369   h, 63%; iv. Ambersep 900 hydroxide form resin, MeOH, 15 min, then $Cu(ClO_4)_2$, MeOH, reflux, 16 h,
370   64%.

371   **Aβ42 Overexpression and purification.** Overexpression and purification of unlabelled Aβ42 was
372   performed according to Walsh and colleagues[34]. Briefly, large cultures of *Escherichia coli* BL21 Gold
373   (DE3) were incubated at 37 °C with shaking, induced with 0.5 mM IPTG and harvested by centrifugation.
374   Purification involved a series of sonication and centrifugation steps followed by resuspension of
375   inclusion bodies in 8M urea. Anion exchange chromatography using diethylaminoethyl cellulose beads
376   was performed and protein eluted with increasing concentrations of NaCl (up to 150 mM). Aβ42 elution
377   was assessed by electrophoresis, using by Novex™ 10–20% Tricine SDS-PAGE gels. Fractions
378   containing elevated levels of Aβ42 were combined and filtered through a 30 kDa molecular mass cut-
379   off centrifugal filtration device (Amicon® Ultra-15). The combined sample was concentrated using a 3
380   kDa molecular mass cut-off centrifugal filtration device (Amicon® Ultra-15), snap frozen, lyophilised and
381   stored at –20 °C. [15]N Aβ42 expression was performed according to Habchi and colleagues[18], with
382   purification as above.

383   **Size exclusion chromatography.** An aliquot of lyophilised Aβ42 protein was solubilised in 6 M GuHCl
384   until no large aggregates were visible. The sample was centrifuged at ~3300 x *g* for 3 min, bath

385 sonicated for 5 min in ice-water and centrifuged again at 16000 x g for 10 min at 4 °C. 500 μL of sample
386 was drawn up carefully with a syringe and loaded onto a Superdex™ 75 Increase 10/300 GL size
387 exclusion column running on an ÄKTA FPLC system. Protein was eluted at 0.5 mL/min in 50 mM
388 ammonium acetate pH 8.5. Fractions (0.5 mL) were collected in Protein LoBind Eppendorf tubes and
389 immediately placed on ice. Fractions were analysed for Aβ42 content using SDS-PAGE. Concentration
390 was measured via spectrophotometer (ε275 = 1450). Fractions containing Aβ42 were combined and
391 either used immediately or snap frozen and lyophilised.

392 **Thioflavin T assays.** Protein samples (Aβ42) were prepared in triplicate in non-binding 96-well half
393 area plates (Corning 3881) in 25 mM or 50 mM NaH_2PO_4 pH 7.4, 40 μM ThT to a final volume of 80 μL.
394 Plate preparation was performed at 4 °C to minimise aggregation. Samples were incubated at 37 °C in
395 a POLARstar Omega microplate reader (BMG Labtech), with excitation at 440 nm and the fluorescence
396 emission recorded at 480 nm under quiescent conditions.

397 **Seeding.** Seeds were prepared by incubating 10 μM Aβ42 in 50 mM NaH_2PO_4, pH 7.4 at 37 °C for 5 h.
398 Protein solution was subject to 6 x 10 s sonication with 20 s rest on ice between cycles. The seeds were
399 maintained on ice and used immediately.

400 **Enhanced BCA assay details.** Kinetic assays were run to completion as judged by the plateau in ThT
401 fluorescence (~5 h). Contents of wells were removed and centrifuged at 16000 x g for 10 min to pellet
402 fibrils and aggregates. Protein concentration was determined using a Pierce® Bicinchoninic Acid Protein
403 Assay Kit according to manufacturer's enhanced protocol. Monomeric Aβ42 and compounds alone
404 were used as controls.

405 **TEM.** Samples were prepared on carbon-coated copper grids (200 mesh) with formvar support film
406 (ProSciTech Pty Ltd.) that had been exposed to UV light (230 nm) for 10 min before sample application
407 and stained with 2% aqueous uranyl acetate solution. Samples were examined with a FEI Tecnai T12
408 electron microscope operating at 120 kV and images captured with a Veleta CCD camera and
409 processed using RADIUS 2.0 imaging software (EMSIS GmbH).

410 **Preparation of Aβ42 for cell assay and NMR.** Lyophilised, purified protein was resuspended in HFIP
411 at 1 mg/mL and incubated for 30 min at room temperature. The protein was snap frozen, lyophilised,
412 and stored at –80 °C until use.

413 **Cell Culture and Differentiation.** SH-SY5Y cells were cultured in in Dulbecco's Modified Eagle
414 Medium: Nutrient Mixture F-12 (DMEM/F12; Invitrogen, Carlsbad, CA, USA) supplemented with 10%
415 fetal bovine serum (FBS; Gibco, Uxbridge, UK) at 37 °C and 5% CO_2. Cells were fed every 2-3 days
416 and passaged using Trypsin-EDTA (0.25%). Cells were detached using Trypsin-EDTA, centrifuged (5
417 min, 125 x g), counted and then plated in a Cell-bind 96-well plate at a density of 0.5×10^4 cells/well in
418 10 μM all-trans retinoic acid (RA; Sigma-Aldrich) in DMEM/F12 with 10% FBS. Media was replaced
419 daily for 4 days (RA is light sensitive, so all steps involving RA were completed in the dark). After a 4-
420 day incubation with RA, media was switched to DMEM/F12 (no serum) with 50 ng/mL BDNF (Sigma-
421 Aldrich) for 3 days. After a total of 7 days of differentiation the cells were used for the experiments.

422 **Aβ42 preparation, compound treatment and CellTiter-Blue® viability assay.** 24 h prior to the cells
423 finishing differentiation, an aliquot of Aβ42 was centrifuged at 16,000 x g for 10 min and dissolved in
424 PBS at 200 μM, then diluted to 20 μM in DMEM/F12 with 10% FBS. The solution was stored in the
425 incubator (37 °C, 5% CO_2) in a low-bind Eppendorf to promote Aβ42 fibrillization. After cell
426 differentiation was complete, for the Aβ42 monomeric preparation, a second aliquot of Aβ42 was
427 centrifuged at 16,000 x g for 10 min, dissolved in PBS at 200 μM and immediately diluted to a final
428 concentration of 20 μM in DMEM/F12 (with 10% FBS). Experimental compounds (10 μM, 0.1%) or
429 DMSO control were added to the fibrillar or monomeric Aβ42. Differentiation media was aspirated,
430 100 μL of each condition added to the cells and incubated for 24 h (37 °C, 5% CO_2). In the monomeric
431 preparation, the time between dissolving the Aβ42 and applying onto the cells was minimised (less than
432 2 min total). After 24 h, CellTiter-Blue® (CTB; Promega G8080) (20 μL/well) was added and incubated

13

433 for 4 h. The fluorescent emission at 590 nm was measured using a POLARstar Omega microplate-
434 reader (BMG Labtech); viable cells metabolise this agent and reduce it to a fluorescent compound.

435 **Statistical Analysis.** One-way ANOVA (analysis of variance) followed by a Bonferroni's multiple
436 comparisons test was used to determine the differences between mean CTB values of differentiated
437 SH-SY5Y cells treated with Aβ42 and/or test compounds relative to vehicle control. Significance
438 threshold was defined as $p < 0.05$.

439 **Kinetic analysis.** The kinetic data obtained in ThT assays were analysed using the online fitting
440 software AmyloFit, following the cited protocol[43]. The model 'secondary nucleation dominated,
441 unseeded' was used, with the reaction orders set to 2 as typical for Aβ42 and under the constraint of
442 allowing deviations from the unperturbed kinetics in only one parameter at a time to investigate which
443 microscopic step or which species of the aggregation mixture was most likely affected by the inhibitors.
444 Repeats of the experiment were analysed separately and combined at the end to estimate uncertainty.

445 K_d **determination.** To determine the value of the dissociation constant, K_d, between free monomer and
446 inhibitor, a one-to-one binding was assumed and the free monomer concentration, m, expressed as a
447 function of the total inhibitor concentration, I_{tot}, the total monomer concentration, m_{tot}, and K_d,

448 $$m = \frac{-I_{tot} + m_{tot} - K_d + \sqrt{(I_{tot} - m_{tot} + K_d)^2 + 4 K_d m_{tot}}}{2}.$$

449 The free monomer concentration was estimated as the effective monomer concentration in the kinetic
450 assays or the relative one-dimensional 1H NMR signal, respectively. Likelihoods were calculated using
451 grid approximations, under the assumption of Gaussian noise.

452 **NMR / K_d Analysis.** All NMR data were collected at 4 °C using unlabelled 10 μM Aβ42 or ^{15}N-labelled
453 Aβ42 in 20 mM NaH_2PO_4 pH 7.0, 10% D_2O, 1 mM DSS. Individual titrations with **C16**, **C17**, **C18** or
454 EGCG were carried out by incubating unlabelled 10 μM Aβ42 with increasing concentrations of the
455 compounds, ranging from 0 to 50 μM. 9 titration points were recorded for each compound. The NMR
456 signals from one-dimensional ^{1}H spectra were used to monitor the binding. Each spectrum was
457 recorded using 512 scans. A ^{1}H–^{15}N heteronuclear single quantum coherence (HSQC) spectrum was
458 also recorded for ^{15}N-labelled Aβ42 in the presence of 10 μM **C16**. The HSQC spectrum was recorded
459 overnight, for 240 scans, with a spectral width of 25 ppm (^{15}N offset at 117.5 ppm). All spectra were
460 obtained using a 18.8 T (800 MHz ^{1}H frequency) Advance III HD Bruker spectrometer equipped with a
461 cryoprobe.

462

463 **Acknowledgements**

475

476 **References**
477

478   1.   I. Benilova, E. Karran and B. De Strooper, *Nature neuroscience*, 2012, **15**, 349-357.
479   2.   S. J. C. Lee, E. Nam, H. J. Lee, M. G. Savelieff and M. H. Lim, *Chemical Society Reviews*, 2017,
480   **46**, 310-323.
481   3.   D. M. Walsh, I. Klyubin, J. V. Fadeeva, W. K. Cullen, R. Anwyl, M. S. Wolfe, M. J. Rowan and D.
482   J. Selkoe, *Nature*, 2002, **416**, 535-539.
483   4.   F. Chiti and C. M. Dobson, *Nature chemical biology*, 2009, **5**, 15-22.
484   5.   J. Fantini, H. Chahinian and N. Yahi, *Protein Science*, 2020, **29**, 1748-1759.
485   6.   P. Jadiya, D. W. Kolmetzky, D. Tomar, A. Di Meco, A. A. Lombardi, J. P. Lambert, T. S. Luongo,
486   M. H. Ludtmann, D. Praticò and J. W. Elrod, *Nature communications*, 2019, **10**, 3885.
487   7.   I. F. Tsigelny, Y. Sharikov, V. L. Kouznetsova, J. P. Greenberg, W. Wrasidlo, T. Gonzalez, P.
488   Desplats, S. E. Michael, M. Trejo-Morales, C. R. Overk and E. Masliah, *Journal of Alzheimer's
489   disease : JAD*, 2014, **39**, 583-600.
490   8.   I. F. Tsigelny, Y. Sharikov, W. Wrasidlo, T. Gonzalez, P. A. Desplats, L. Crews, B. Spencer and
491   E. Masliah, *The FEBS journal*, 2012, **279**, 1000-1013.
492   9.   B. Winner, R. Jappelli, S. K. Maji, P. A. Desplats, L. Boyer, S. Aigner, C. Hetzer, T. Loher, M.
493   Vilar, S. Campioni, C. Tzitzilonis, A. Soragni, S. Jessberger, H. Mira, A. Consiglio, E. Pham, E.
494   Masliah, F. H. Gage and R. Riek, *Proceedings of the National Academy of Sciences*, 2011, **108**,
495   4194-4199.
496   10. B. Zott, M. M. Simon, W. Hong, F. Unger, H.-J. Chen-Engerer, M. P. Frosch, B. Sakmann, D. M.
497   Walsh and A. Konnerth, *Science*, 2019, **365**, 559-565.
498   11. M. Serra-Batiste, M. Ninot-Pedrosa, M. Bayoumi, M. Gairí, G. Maglia and N. Carulla,
499   *Proceedings of the National Academy of Sciences*, 2016, **113**, 10866-10871.
500   12. T. C. T. Michaels, A. Šarić, S. Curk, K. Bernfur, P. Arosio, G. Meisl, A. J. Dear, S. I. A. Cohen, C.
501   M. Dobson, M. Vendruscolo, S. Linse and T. P. J. Knowles, *Nature Chemistry*, 2020, **12**, 445-
502   451.
503   13. S. I. A. Cohen, S. Linse, L. M. Luheshi, E. Hellstrand, D. A. White, L. Rajah, D. E. Otzen, M.
504   Vendruscolo, C. M. Dobson and T. P. J. Knowles, *Proceedings of the National Academy of
505   Sciences*, 2013, **110**, 9758-9763.
506   14. J. E. Gillam and C. E. MacPhee, *Journal of physics. Condensed matter : an Institute of Physics
507   journal*, 2013, **25**, 373101.
508   15. S. Linse, *Biophys Rev*, 2017, **9**, 329-338.
509   16. T. C. T. Michaels, A. Šarić, G. Meisl, G. T. Heller, S. Curk, P. Arosio, S. Linse, C. M. Dobson, M.
510   Vendruscolo and T. P. J. Knowles, *Proceedings of the National Academy of Sciences*, 2020,
511   DOI: 10.1073/pnas.2006684117, 202006684.
512   17. J. Habchi, P. Arosio, M. Perni, A. R. Costa, M. Yagi-Utsumi, P. Joshi, S. Chia, S. I. A. Cohen, M.
513   B. D. Müller, S. Linse, E. A. A. Nollen, C. M. Dobson, T. P. J. Knowles and M. Vendruscolo,
514   *Science Advances*, 2016, **2**, e1501244.
515   18. J. Habchi, S. Chia, R. Limbocker, B. Mannini, M. Ahn, M. Perni, O. Hansson, P. Arosio, J. R.
516   Kumita, P. K. Challa, S. I. A. Cohen, S. Linse, C. M. Dobson, T. P. J. Knowles and M.
517   Vendruscolo, *Proceedings of the National Academy of Sciences*, 2017, **114**, E200-E208.
518   19. R. Limbocker, S. Chia, F. S. Ruggeri, M. Perni, R. Cascella, G. T. Heller, G. Meisl, B. Mannini, J.
519   Habchi, T. C. T. Michaels, P. K. Challa, M. Ahn, S. T. Casford, N. Fernando, C. K. Xu, N. D. Kloss,
520   S. I. A. Cohen, J. R. Kumita, C. Cecchi, M. Zasloff, S. Linse, T. P. J. Knowles, F. Chiti, M.
521   Vendruscolo and C. M. Dobson, *Nature communications*, 2019, **10**, 225.
522   20. M. Ettcheto, A. Cano, P. R. Manzine, O. Busquets, E. Verdaguer, R. D. Castro-Torres, M. L.
523   García, C. Beas-Zarate, J. Olloquequi, C. Auladell, J. Folch and A. Camins, *Molecular
524   neurobiology*, 2020, **57**, 1814-1827.
525   21. R. Cataldi, S. Chia, K. Pisani, F. S. Ruggeri, C. K. Xu, T. Šneideris, M. Perni, S. Sarwat, P. Joshi, J.
526   R. Kumita, S. Linse, J. Habchi, T. P. J. Knowles, B. Mannini, C. M. Dobson and M. Vendruscolo,
527   *Commun Biol*, 2021, **4**, 19-19.

528 22. G. T. Heller, F. A. Aprile, T. C. T. Michaels, R. Limbocker, M. Perni, F. S. Ruggeri, B. Mannini, T.
529   Löhr, M. Bonomi, C. Camilloni, A. De Simone, I. C. Felli, R. Pierattelli, T. P. J. Knowles, C. M.
530   Dobson and M. Vendruscolo, *Science Advances*, 2020, **6**, eabb5924.
531 23. S. I. A. Cohen, P. Arosio, J. Presto, F. R. Kurudenkandy, H. Biverstål, L. Dolfe, C. Dunning, X.
532   Yang, B. Frohm, M. Vendruscolo, J. Johansson, C. M. Dobson, A. Fisahn, T. P. J. Knowles and
533   S. Linse, *Nature Structural & Molecular Biology*, 2015, **22**, 207-213.
534 24. A. Munke, J. Persson, T. Weiffert, E. De Genst, G. Meisl, P. Arosio, A. Carnerup, C. M.
535   Dobson, M. Vendruscolo, T. P. J. Knowles and S. Linse, *Proceedings of the National Academy*
536   *of Sciences*, 2017, **114**, 6444.
537 25. H. Liu, L. Yu, X. Dong and Y. Sun, *Journal of Colloid and Interface Science*, 2017, **491**, 305-312.
538 26. F. L. Palhano, J. Lee, N. P. Grimster and J. W. Kelly, *Journal of the American Chemical Society*,
539   2013, **135**, 7503-7510.
540 27. L. M. Young, J. C. Saunders, R. A. Mahood, C. H. Revill, R. J. Foster, L.-H. Tu, D. P. Raleigh, S. E.
541   Radford and A. E. Ashcroft, *Nature Chemistry*, 2015, **7**, 73-81.
542 28. L. Zhu, Y. Song, P.-N. Cheng and J. S. Moore, *Journal of the American Chemical Society*, 2015,
543   **137**, 8062-8068.
544 29. E. Tamanini, K. Flavin, M. Motevalli, S. Piperno, L. A. Gheber, M. H. Todd and M. Watkinson,
545   *Inorganic Chemistry*, 2010, **49**, 3789-3800.
546 30. J. K.-H. Wong, S. Ast, M. Yu, R. Flehr, A. J. Counsell, P. Turner, P. Crisologo, M. H. Todd and P.
547   J. Rutledge, *ChemistryOpen*, 2016, **5**, 375-385.
548 31. M. Yu, T. M. Ryan, S. Ellis, A. I. Bush, J. A. Triccas, P. J. Rutledge and M. H. Todd, *Metallomics*,
549   2014, **6**, 1931-1940.
550 32. S. L. Risacher, N. Fandos, J. Romero, I. Sherriff, P. Pesini, A. J. Saykin and L. G. Apostolova,
551   *Alzheimer's & dementia (Amsterdam, Netherlands)*, 2019, **11**, 510-519.
552 33. S. Linse, *Methods in molecular biology (Clifton, N.J.)*, 2020, **2141**, 731-754.
553 34. D. M. Walsh, E. Thulin, A. M. Minogue, N. Gustavsson, E. Pang, D. B. Teplow and S. Linse, *The*
554   *FEBS journal*, 2009, **276**, 1266-1281.
555 35. M. Yu, G. Nagalingam, S. Ellis, E. Martinez, V. Sintchenko, M. Spain, P. J. Rutledge, M. H. Todd
556   and J. A. Triccas, *Journal of Medicinal Chemistry*, 2016, **59**, 5917-5921.
557 36. E. House, J. Collingwood, A. Khan, O. Korchazkina, G. Berthon and C. Exley, *Journal of*
558   *Alzheimer's disease : JAD*, 2004, **6**, 291-301.
559 37. M.-C. Lee, W.-C. Yu, Y.-H. Shih, C.-Y. Chen, Z.-H. Guo, S.-J. Huang, J. C. C. Chan and Y.-R. Chen,
560   *Scientific Reports*, 2018, **8**, 4772.
561 38. M. Mold, L. Ouro-Gnao, B. M. Wieckowski and C. Exley, *Scientific Reports*, 2013, **3**, 1256.
562 39. C. Haass and D. J. Selkoe, *Nature Reviews Molecular Cell Biology*, 2007, **8**, 101-112.
563 40. J. Krishtal, O. Bragina, K. Metsla, P. Palumaa and V. Tõugu, *PLOS ONE*, 2017, **12**, e0186636.
564 41. S. I. Cohen, M. Vendruscolo, M. E. Welland, C. M. Dobson, E. M. Terentjev and T. P. Knowles,
565   *The Journal of chemical physics*, 2011, **135**, 065105.
566 42. T. P. J. Knowles, C. A. Waudby, G. L. Devlin, S. I. A. Cohen, A. Aguzzi, M. Vendruscolo, E. M.
567   Terentjev, M. E. Welland and C. M. Dobson, *Science*, 2009, **326**, 1533-1537.
568 43. G. Meisl, J. B. Kirkegaard, P. Arosio, T. C. Michaels, M. Vendruscolo, C. M. Dobson, S. Linse
569   and T. P. Knowles, *Nature protocols*, 2016, **11**, 252-272.
570 44. J. M. Lopez del Amo, U. Fink, M. Dasari, G. Grelle, E. E. Wanker, J. Bieschke and B. Reif,
571   *Journal of molecular biology*, 2012, **421**, 517-524.
572 45. J. Roche, Y. Shen, J. H. Lee, J. Ying and A. Bax, *Biochemistry*, 2016, **55**, 762-775.
573 46. J. R. Horsley, B. Jovcevski, K. L. Wegener, J. Yu, T. L. Pukala and A. D. Abell, *The Biochemical*
574   *journal*, 2020, **477**, 2039-2054.
575 47. J. Bieschke, J. Russ, R. P. Friedrich, D. E. Ehrnhoefer, H. Wobst, K. Neugebauer and E. E.
576   Wanker, *Proceedings of the National Academy of Sciences*, 2010, **107**, 7710-7715.
577 48. D. E. Ehrnhoefer, J. Bieschke, A. Boeddrich, M. Herbst, L. Masino, R. Lurz, S. Engemann, A.
578   Pastore and E. E. Wanker, *Nature Structural & Molecular Biology*, 2008, **15**, 558-566.

579 49.   M. Spain, J. K. H. Wong, G. Nagalingam, J. M. Batten, E. Hortle, S. H. Oehlers, X. F. Jiang, H. E.
580   Murage, J. T. Orford, P. Crisologo, J. A. Triccas, P. J. Rutledge and M. H. Todd, *Journal of*
581   *Medicinal Chemistry*, 2018, **61**, 3595-3608.
582 50.   M. Yu, Q. Yu, P. J. Rutledge and M. H. Todd, *ChemBioChem*, 2013, **14**, 224-229.

583